J Mater Sci (2006) 41:7730–7740
DOI 10.1007/s10853-006-0736-x

Kinematics, dynamics, and microstructural effects of grain boundary junctions

G. Gottstein · D. A. Molodov · L. S. Shvindlerman

Received: 28 February 2006 / Accepted: 28 July 2006 / Published online: 24 October 2006

Abstract The impact of grain boundary junctions on the coarsening of grain boundary networks is reviewed. The various kinds of junctions are introduced, the dynamic steady state configurations are defined, and their equation of motion is derived. It is shown that a limited junction mobility can effectively hinder grain growth, in particular in fine grained materials. The theory is substantiated by computer simulations and supported by experimental results. We propose to utilize Grain Boundary Junction Engineering as an effective tool for microstructure control.

Introduction

Real materials are generally composed of a large number of small crystallites. The contact surface of adjacent grains is referred to as grain boundary. The arrangement of grain boundaries of a polycrystal comprises a 3D contiguous network which requires that grain boundaries form junctions, i.e. triple lines and quadruple points. Traditionally, the evolution and properties of the granular assembly of a polycrystal are described entirely in terms of grain boundary characteristics while the junctions are tacitly assumed not to affect microstructure development and thus, can be disregarded. That is particularly reflected by the well known von Neumann–Mullins relation. According to this approach, grain boundary junctions do not affect grain boundary motion, and their role in grain growth is reduced to maintain the thermodynamically prescribed equilibrium angles at the locations where boundaries meet.

In the current study experimental data, theoretical concepts, and computer simulations of grain boundary systems moving with the junctions are considered with respect to the process of grain growth in 2D systems, in particular with regard to the controlling kinetics.

In the following, we will demonstrate that grain boundary junctions constitute defects on their own with specific thermodynamic and kinetic properties and that they do influence the kinematics and dynamics of grain microstructure evolution and thus, affect the mechanical, physical, and chemical properties of a processed polycrystalline material. This paper reviews recent progress in the field of grain boundary junction behavior. For details the reader is referred to references [1–5].

Types and kinematics of grain boundary junctions

Geometrical characterization

There are two fundamental types of grain boundary junctions in bulk polycrystalline materials, triple lines, and quadruple points. A triple line forms where 3 grain boundaries meet, whereas a quadruple point is the geometrical location where four grains come into contact. There is a large variety of potential triple lines

G. Gottstein (✉) · D. A. Molodov · L. S. Shvindlerman
Institut für Metallkunde und Metallphysik, RWTH Aachen, Kopernikusstr. 14, Aachen D-52056, Germany
e-mail: gottstein@imm.rwth-aachen.de

L. S. Shvindlerman
Institute of Solid State Physics, Russian Academy of Sciences, Chernogolovka, Moscow Distr. 142432, Russia

and quadruple points in polycrystalline materials since their geometry is determined by the constituting grain boundaries, each of which has five degrees of freedom. Hence, a triple line is defined by 12 independent geometrical parameters; a quadruple point requires up to 21 quantities for a unique geometrical characterization. Despite this large parameter space of potential triple lines and quadruple points, there are only very few configurations of boundaries that will cause a steady state motion of the connected boundary systems. Such configurations will be introduced and discussed in the following.

Kinematics of grain boundary junctions

Triple lines

Essentially we distinguish two fundamental types of triple junctions with steady state kinematics, namely a junction with a specific shrinking grain (Fig. 1a) and a specific growing grain (Fig. 1b). For steady state motion the boundaries have to obey special boundary conditions with respect to grain boundary surface tension and mobility.

Below, we will derive the equation of motion for such configurations.

To begin with, we consider a system of three grain boundaries with a common triple junction as depicted in Fig. 1a. The system is understood to be quasi-2D, i.e. the boundaries are assumed to run straight through the sample thickness. Two of the boundaries are curved, which results in a force on the entire boundary–junction-system. The convex shape of the boundaries corresponds to the curvature of grains with less than six sides in a polycrystal. Hence, this geometry is representative for 2D grains with $n < 6$, where n is the number of sides of a grain.

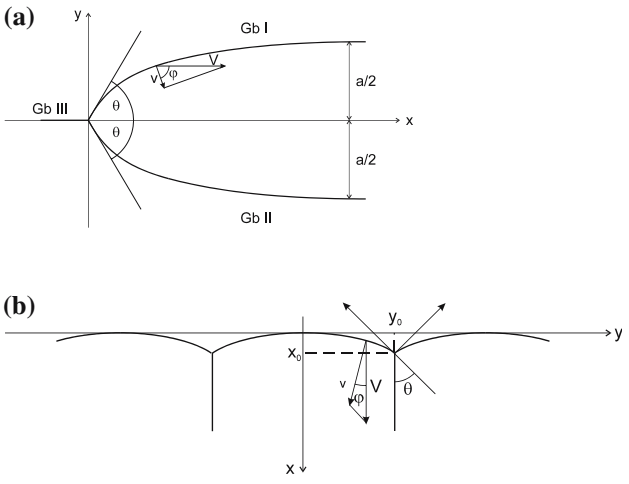

Fig. 1 (**a**) Configuration of grain boundaries at a triple junction during steady state motion for $n < 6$. (**b**) Configuration of grain boundaries at triple junctions during steady state motion for $n > 6$

The normal velocity of a curved boundary is given by

$$v = m_{\mathrm{b}}\gamma K \tag{1}$$

where K is the curvature, m_{b} and γ are the mobility and energy of the boundary, respectively.

During steady state motion of the whole system the horizontal velocity V is related to the normal displacement rate v

$$v = V\cos\varphi = V\frac{y'}{\left(1+(y')^2\right)^{1/2}} \tag{2}$$

where $y(x)$ is the shape of the upper part of the curved boundary in Fig. 1a (due to the mirror symmetry of the problem relative to the x-axis, the shape of the lower boundary is the negative equivalent).

From Eqs. (1) and (2) and taking into account the expression for the curvature K

$$K = -\frac{y''}{\left(1+(y')^2\right)^{3/2}} \tag{3}$$

we obtain the equation for the shape of the moving grain boundary

$$y'' = -\frac{V}{m_{\mathrm{b}}\gamma}y'\left(1+(y')^2\right) \tag{4}$$

With the boundary conditions $y(0) = 0$, $y(\infty) = a/2$, $y'(0) = \tan\theta$, Eq. (4) has the solution

$$y(x) = \xi\arccos\left(\mathrm{e}^{-x/\xi+c_1}\right) + c_2 \tag{5}$$

$\xi = a/2\theta, c_1 = \ln(\sin\theta), c_2 = -\xi(\pi/2-\theta)$. The angle θ is the angle at the tip of triple junction (Fig. 1).

With Eq. (5) the local grain boundary velocity can be calculated from Eq. (2). The meaning of the length a and the angle θ is clear from Fig. 1a.

A driving force $\gamma(2\cos\theta - 1)$ acts on the triple junction from the curved boundaries. Introducing the mobility of the triple junction m_{Tj}, its velocity reads

$$V_{\mathrm{Tj}} = m_{\mathrm{Tj}}\,\gamma(2\cos\Theta - 1) \tag{6}$$

Note that the ratio $m_{\mathrm{b}}/m_{\mathrm{Tj}}$ has the dimension of a length.

The horizontal velocity V of steady state motion of the grain boundary system is

$$V = \frac{2\theta m_b \gamma}{a} \tag{7}$$

From the condition $V = V_{Tj}$ the steady state value for the angle Θ can be found from the equation

$$\frac{2\theta}{2\cos\theta - 1} = \frac{m_{Tj} a}{m_b} = \Lambda \tag{8}$$

This defines the criterion Λ, which determines the migration behavior of the connected boundary system, as will be discussed below.

If a triple junction is perfectly mobile and does not drag grain boundary motion, then $\Lambda \to \infty$ and $\theta \to \pi/3$, i.e. the equilibrium angle at a triple junction in the uniform grain boundary model. In contrast, however, if the mobility of the triple junction is relatively low, i.e. $m_{Tj} a \ll m_b$ then $\theta \to 0$ [6]. It is particularly emphasized that the angle θ is comprehensively defined by the dimensionless parameter Λ, which, in turn, is a function of both the ratio of triple junction and grain boundary mobility, and the grain size. Thus, a ''triple junction of low mobility'' means a ''small value of Λ''.

Experimental investigations on such grain boundary systems (Fig. 2) revealed that triple junctions can have a low mobility [7–9]. In particular, it the vertex angle θ at the triple junction can markedly deviate from the equilibrium value, in case of a low triple junction mobility. In fact, a transition from triple junction kinetics to grain boundary kinetics was observed (Fig. 2).

The steady state motion of a grain boundary system shown in Fig. 1b can be treated by analogy. It represents the case of 2D grains with $n > 6$. Again, we assume uniform grain boundary properties and quasi-2D geometry. The steady state motion of this assembly is determined by the set of Eqs. (1), (2), and (3) only with different boundary and initial conditions; $y'(0) = \infty$, $y'(x_0) = \tan\theta$, $y(0) = 0$ to yield

$$y(x) = -\frac{x_0}{\ln\sin\theta} \arccos\left(e^{\frac{x}{x_0}\ln\sin\theta}\right) \tag{9}$$

From the imbalance of surface tensions at the triple junction follows a triple junction migration rate

$$V_{Tj} = m_{Tj}\,\gamma(1 - 2\cos\theta) \tag{10}$$

The boundary curvature causes a horizontal steady state velocity of the boundary system

$$V = -\frac{m_b \gamma}{x_0} \ln\sin\theta \tag{11}$$

The length $0 - x_0$ represents essentially the grain size (Fig. 1b). From the condition $V_{Tj} = V$ we obtain for $n > 6$

$$-\frac{\ln\sin\theta}{1 - 2\cos\theta} = \frac{m_{Tj} x_0}{m_b} = \Lambda \tag{12}$$

Obviously, for $\Lambda \gg 1$, when the boundary mobility determines the kinetics of the system the angle θ tends to its equilibrium value ($\pi/3$). Again, the angle θ changes when a low mobility of the triple junction starts to drag the motion of the boundary system. However, as apparent from Eq. (12) and Fig. 1b, in this case the steady state value of the angle θ is larger than in static equilibrium.

As shown in [1–8], the mobility of grain boundary junctions is finite; the activation enthalpy of it is, as a rule, essentially higher than the activation enthalpy of grain boundary mobility. So, under definite conditions, particularly at low temperatures, grain boundary junctions can drag grain boundary motion and, consequently, slow down grain growth. Another source of junction drag results from topology, because the mere existence of grain boundary junctions hinders grain boundary motion. Contrary to other obstacles to grain boundary motion, junctions cannot be circumvented but must be dragged along. That is why junction drag can be stronger than impurity and particle drag.

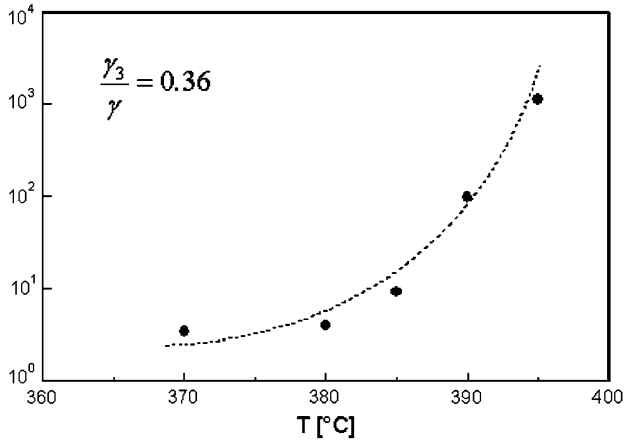

Fig. 2 Measured temperature dependence of the criterion Λ for Zn tricrystals [7]

Quadruple junctions

A basic type of quadruple junction with steady state kinetic behavior is sketched in Fig. 3. It is composed of

four grains which touch at the point O. The lines in this figure represent triple junction lines.

The shape of the triple lines resembles the shape of a grain boundary in a tricrystal comprising a model grain boundary system with a triple junction; far from the quadruple point all three boundaries are rectilinear and parallel each to other.

In such a configuration motion proceeds under the action of the triple junction line tension γ^1. We will consider this problem in the framework of a uniform triple junction model, i.e. all triple lines possess constant and uniform line tensions and mobilities irrespective of the misorientation of the adjacent grains and the crystallographic orientation of the boundaries.

The given assumptions require symmetry with respect to any plane that contains the curved triple line (Fig. 3). The velocity of the triple junction defines the differential equation of the shape $y(x)$ of a moving triple junction. The velocity of normal motion of a triple junction element is

$$v = m_{\mathrm{Tj}}\gamma^1\kappa \tag{13}$$

where

$$\kappa = -y''\left[1 + (y')^2\right]^{-3/2} \tag{14}$$

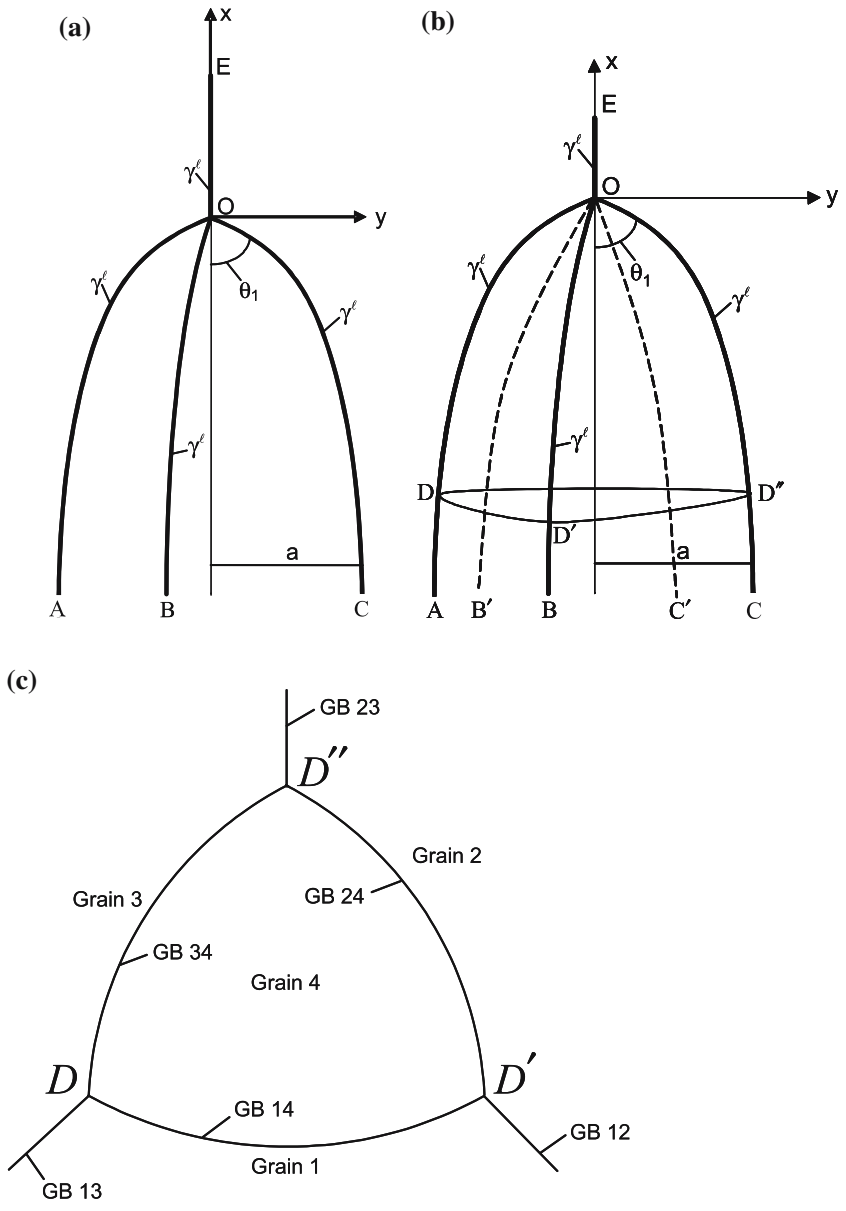

Fig. 3 (**a**) Four grain arrangements with four triple lines (OA, OB, OC, OE) and one quadruple point at O. The angle θ_1 is the vertex angle of a triple line at the quadruple junction, a is the (half) dimension of the grain bounded by the OA, OB, and OC. (**b**) Arrangement of a four grain system: DD′D″ denotes a plane perpendicular to the x-axis that intersects all four grains (see Fig. 3c). (**c**) Section through the four grain arrangement shown in Fig. 3b. The lines DD′, D′D″, and D″D denote the grain boundaries between the three exterior grains and the interior grain

is the curvature of the triple line element. During steady-state motion the horizontal velocity V is constant (Fig. 4)

$$v = V\cos\theta_1 = Vy'\left[1+(y')^2\right]^{-1/2} \tag{15}$$

Hence,

$$y'' = -\frac{V}{m_{\mathrm{Tj}}\gamma^1}y'\left[1+(y')^2\right] \tag{16}$$

with the boundary conditions $y(0) = 0$, $y(\infty) = a/2, y'(0) = \tan\theta_1$, where $y(x)$ is the shape function of the triple line, θ_1 is the angle at the tip of the triple junctions at the quadruple point (see Fig. 3).

For derivation of the force F acting on the quadruple point, let us consider a plane that contains the triple line OC and the x-axis (Figs. 3a, 4). The components of all triple line tensions acting on the quadruple junction in this plane is $F = 2\gamma^1\cos 60\cos\theta_1 + \gamma^1\cos\theta_1 - \gamma^1$. Then, the velocity of the quadruple point motion reads:

$$\begin{aligned} V_{qp} &= m_{qp}[2\gamma^1\cos 60\cos\theta_1 + \gamma^1\cos\theta_1 - \gamma^1] = \\ &= m_{qp}\gamma^1[2\cos 60\cos\theta_1 + \cos\theta_1 - 1] \end{aligned} \tag{17}$$

where m_{qp} is the mobility of the quadruple point.

Eqs. (3) and (4) define the problem comprehensively. Integration of Eq. (3) yields the shape of a steady-state moving triple junction system with a quadruple point. It reads

$$y(x) = \varsigma\arccos(\mathrm{e}^{-x/\varsigma+C_1}) + C_2 \tag{18}$$

$\varsigma = \frac{a}{2\theta_1}, C_1 = \frac{1}{2}\ln(\sin\theta_1)^2, C_2 = \varsigma(\pi/2-\theta_1)$.

Evidently, a grain boundary system with a quadruple point can move in steady state.

The horizontal velocity V of steady-state motion of the triple junction system is

$$V = \frac{2\theta_1 m_{\mathrm{Tj}}\gamma^1}{a} \tag{19}$$

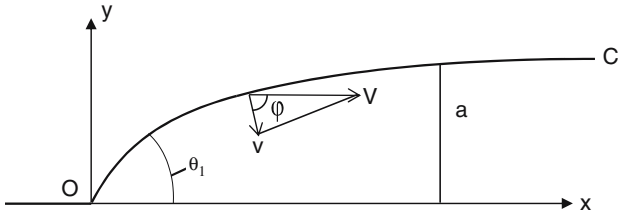

Fig. 4 Cross-section parallel to the grain boundary triple line OC in Fig. 3

From the condition $V = V_{\mathrm{qp}}$ for triple junction and quadruple point motion (Eqs. (16) and (17)) we arrive at the steady-state value of the angle θ_1:

$$\Lambda_{\mathrm{qp}} = \frac{m_{\mathrm{qp}}a}{m_{\mathrm{Tj}}} = \frac{2\theta_1}{\cos\theta_1(2\cos 60+1)-1} = \frac{2\theta_1}{2\cos\theta_1 - 1} \tag{20}$$

If a quadruple point is perfectly mobile and does not drag grain boundary motion, then $\Lambda_{\mathrm{qp}} \to \infty$ and $\theta_1 \to \pi/3$, which is the equilibrium angle between quadruple point and triple junction line in the uniform boundary and triple line model. By contrast, for a low mobility of the quadruple point $m_{\mathrm{qp}}a \ll m_{\mathrm{Tj}}$, then $\theta_1 \to 0$. The angle θ_1 is unambiguously defined by the dimensionless parameter Λ_{qp}, which, in turn, is a function of both the ratio of quadruple point and triple junction mobility, and of the grain size.

Effect of junctions on microstructure evolution

Since quadruple junctions are difficult to visualize and even more difficult to investigate experimentally, because they are true 3D objects which are hard to reveal in non-transparent materials like metals, we will confine our analysis in the following to triple lines in quasi-2D configurations as depicted in Fig. 1a.

A fundamental equation that relates the growth rate of 2D grains with their topology is the Von Neumann–Mullins (vNM) relation [10, 11]. It was derived for grain boundaries of uniform energy σ and mobility m_{b} and equilibrium triple junctions

$$\frac{\mathrm{d}S}{\mathrm{d}t} = \frac{\pi}{3}m_{\mathrm{b}}\,\gamma(2\pi - n_3^{\pi}) = \frac{\pi}{3}m_{\mathrm{b}}\gamma(n-6) \tag{21}$$

If the contact angle at the triple junctions deviates from the equilibrium value $2\pi/3$, the VNM relation has to be modified

$$\dot{S} = -\frac{A_{\mathrm{b}}}{1+\frac{1}{\Lambda}}[2\pi - n(\pi - 2\theta)] \tag{22}$$

where $A_{\mathrm{b}} = m_{\mathrm{b}}\gamma$ is the reduced grain boundary mobility, γ is the grain boundary surface tension.

The rate of grain area change $\dot{S}$ for grains of different topological classes depends on the parameter Λ. For grains with $n < 6$ a limited triple junction mobility lowers the steady state value of the angle θ and the shrinking rate decreases. For grains with $n > 6$ triple junction drag increases the angle θ and also reduces the growth rate of such grains. In other words, micro-

structural evolution is slowed down by triple junction drag for any n-sided grain.

In the classical vNM approach (i.e. $\Lambda \to \infty$) the topological class n^* of stable grains, i.e. $\dot{S}(n^*) = 0$, is $n^* = 6$. For finite Λ n^* is not constant any more but depends on Λ [3].

For $n < 6$

$$n_{\mathrm{L}}^* = \frac{2 + \sqrt{3}\Lambda}{1 + \frac{\sqrt{3}}{6}\Lambda} \tag{23}$$

and for $n > 6$:

$$n_{\mathrm{H}}^* = \frac{6}{1 - \frac{6}{\pi\Lambda B}} \tag{24}$$

where $B = -\frac{\sqrt{3}}{\ln \sin \pi/3}$. Grains with a number of sides $n_{\mathrm{L}}^* < n < n_{\mathrm{H}}^*$ become locked and can neither grow nor shrink [1, 3]. Since $n_{\mathrm{L,H}}^*$ is distinctly different from the vNM limit $n^* = 6$ for small Λ the influence of these locked grains may be very important for the microstructural stability, in particular of ultra fine grained and nanocrystalline materials.

When the triple junction influence is tangibly large, but nevertheless, grain growth can still be considered as governed by grain boundary motion, the average grain area $\langle S \rangle$ changes practically linear with time, however, the rate of grain area changes $\dot{S}$, contrary to the vNM relation, is defined not only by the topological class n but by the criterion Λ as well: $\dot{S} = \dot{S}(n, \Lambda)$ (Figs. 5,6).

It is emphasized that triple junction drag does not only slow down grain microstructure evolution, but changes the final distribution of grains of different topological classes as well [12]

$$\frac{\mathrm{d}\Lambda}{\mathrm{d}t} = -\tilde{\beta}\frac{2\pi - n(\pi - 2\theta)}{\Lambda} \tag{25}$$

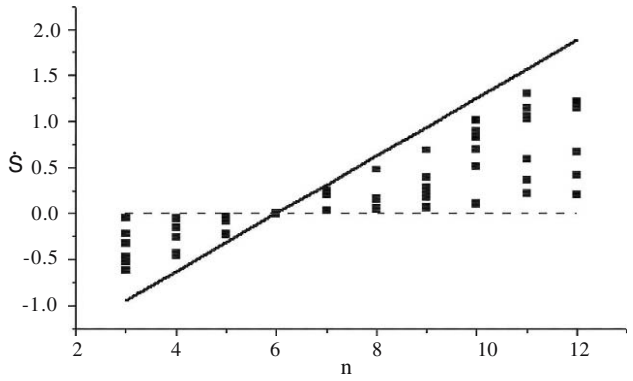

Fig. 5 Simulation result for $0.1<\Lambda<1.0\dot{S}$ as function of n for $0.1 < \Lambda < 10$. Solid squares are the results of computer experiment, the line is the von Neumann–Mullins relation

where $\tilde{\beta}$ is a kinetic coefficient. For rather large Λ the derivative $\frac{\mathrm{d}\Lambda}{\mathrm{d}t}$ approaches:

$$\frac{\mathrm{d}\Lambda}{\mathrm{d}t} = \beta\frac{n-6}{\Lambda} \tag{26}$$

with $\beta = \tilde{\beta}\pi/3$.

Eqs. (25) and (26) demonstrate that triple junction drag affects the growth of grains of different topological classes n markedly different.

If triple junction drag grows very strong, the triple junctions eventually determine the kinetics. This will be referred to as triple junction kinetics. Under triple junction kinetics grains are bordered by straight lines, i.e. the grain boundaries in a 2D polycrystal represent a system of polygons. Moreover, the system of polygons tends to approach a system of equilateral polygons. The only exception is the triangle which will collapse without transforming into a regular polygon.

The rate of grain area change of a regular n-sided polygon with an interior and exterior circle of radius $\tilde{r}$ and $\tilde{r}$, respectively, under triple junction kinetics can be described by [3]

$$\begin{aligned}\dot{S} &= -m\gamma n\tilde{R}\sin\left(\frac{2\pi}{n}\right)\left[2\sin\left(\frac{\pi}{n}\right) - 1\right] \\ &= -2m_{\mathrm{tj}}\gamma n\tilde{r}\sin\left(\frac{\pi}{n}\right)\left[2\sin\left(\frac{\pi}{n}\right) - 1\right]\end{aligned} \tag{27}$$

Computer simulations

In the VNM approach only a single grain and its behavior is considered in an unspecified, i.e. average environment. To study the effect of discrete granular arrangements we employed computer simulations of 2D grain growth. Curvature and boundary tension driven grain growth is conveniently represented by a (virtual) vertex model [13–15]. In such model, the driving force is the net grain boundary surface tension at a vertex. A vertex can be a triple junction or any corner on a polygonized grain boundary. In a time increment, the equation of motion is solved simultaneously for all vertices. Each vertex is assigned a mobility so that different mobilities for triple junctions and boundaries can easily be implemented.

In Fig. 7 the simulated evolution of the microstructure of a 2D polycrystal is presented at various stages of grain growth. As apparent from Fig. 7a for unconstrained grain boundary motion the grains are bordered by curved boundaries. The dependence of the mean grain area on time, and especially the

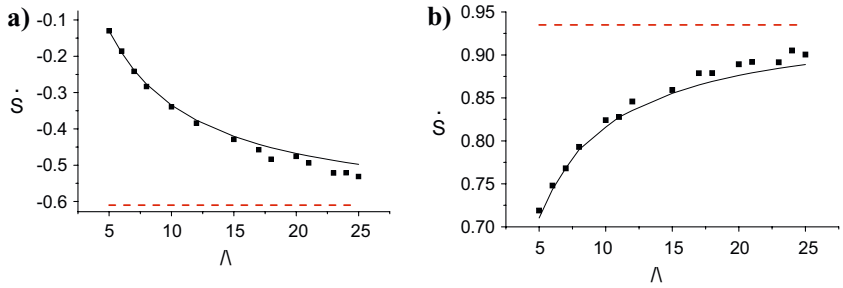

Fig. 6 The rate of grain area change $\dot{S}$ as a function of Λ (**a**) for grains with $n = 4$. Filled squares are the results of computer simulations. The solid line represents the theoretical prediction for intermediate kinetics ($5 < \Lambda < 25$), the dotted line corresponds to the von Neumann–Mullins relation

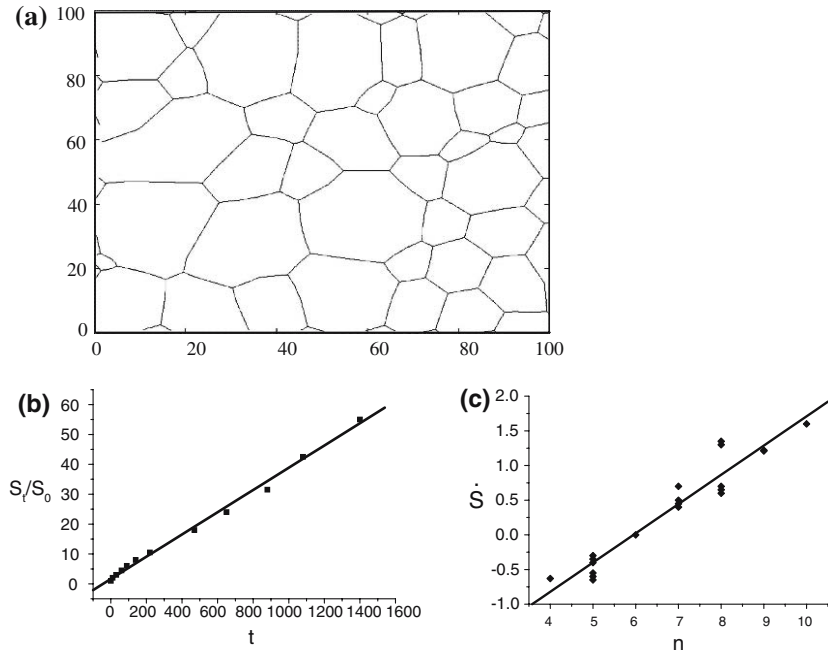

Fig. 7 (**a**) Simulation results for a 2D polycrystal for grain boundary kinetics ($\Lambda \to \infty \varnothing$). (**a**) Microstructure at $S(t)/S_0 = 17.2$; (**b**) normalized area $S(t)/S_0$ versus time t; (**c**) $\dot{S}$ as function of n

dependence of the rate of grain area change $\dot{S}$ vs the topological class n of a grain are shown in Fig. 7b,c. They reflect all features that are peculiar to a ''von Neumann–Mullins polycrystal'': $\langle S \rangle$ increases linearly with annealing time; the rate of grain area change $\dot{S}$ is linear in n, and the line $\dot{S}(n)$ intersects the axis n at $n = 6$, i.e. $\dot{S} = 0$ at $n = 6$. The slope of the line $\dot{S}(n) = \frac{\pi m_b \gamma_b}{3}$ is as predicted by the vNM relation. In essence, for boundary controlled grain growth of a homogeneous system the vNM approach is convincingly reproduced.

In order to study the effect of triple junction mobility on grain growth, two situations were considered. The first case related to the kinetics, when the triple junction influence is tangibly large, but nevertheless, the evolution of the system can be described as a result of curvature driven grain boundary motion. This causes the boundaries to become much more straight (Fig. 8a). When Λ is still relatively large, $0.4 \le \Lambda \le 5.0$, the mean grain area $\langle S \rangle$ changes linearly with time t, which reflects the nature of the controlling grain boundary kinetics of the system at this stage (Fig. 8b). However, the quantitative variation of the rate of grain area change $\dot{S}$ on topological class n, which is a straight line for pure grain boundary kinetics (Fig. 7c) is transformed to an area under the constraint of a finite triple junction mobility (Fig. 5). For all topological classes a large scatter of $\dot{S}(n)$ is observed. While for unconstrained grain boundary kinetics (infinite junction mobility) $\dot{S}$ is a function of n only, for a system with finite junction mobility $\dot{S}$ becomes a function of both n and Λ, $\dot{S} = \dot{S}(n, \Lambda)$ (Fig. 5). The straight line in Fig. 5, which describes the vNM relationship, has the slope $\frac{\pi m_b \gamma_b}{3}$ and $\dot{S}(n = 6) = 0$.

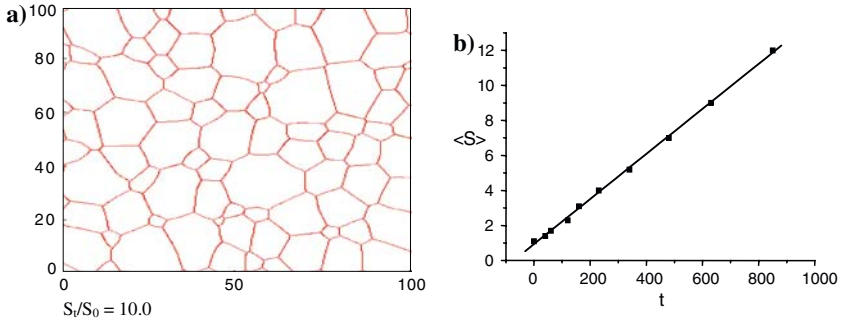

Fig. 8 Simulation result for $0.1 < \Lambda < 1.0$. (**a**) Microstructure at $S(t)/S_0 = 10.0$; (**b**) average area $< S >$ versus time t; $\dot{S}$ as function of n for is given in Fig. 5. Solid squares are the results of computer experiments, the line represents the von Neumann–Mullins relation

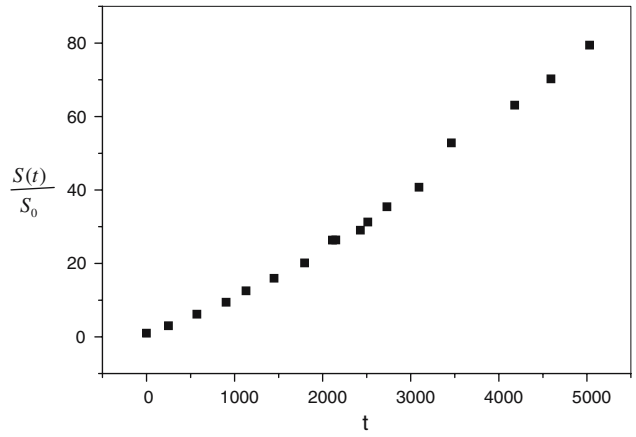

Fig. 9 Grain size versus time for $0.01 < \Lambda < 1.0$

As the parameter Λ decreases the influence of triple junction drag becomes obvious not only in the $\dot{S} - n$ diagram, but also in a change of the dependency $\langle S \rangle$(t) (Fig.9).

The dependency $\dot{S}_n(\Lambda)$ clearly demonstrates that for a given n, $\dot{S}(\Lambda)$ is not represented by a point anymore, but by a line (Fig.10). We note the good agreement between the computer experiment and theory. The expressions

$$\lambda_{n<6} \equiv \frac{\dot{S}^{\mathrm{Tj}}_{n<6}}{\dot{S}_{n<6}} \cong \frac{n\frac{6+\Lambda\sqrt{3}}{2+\Lambda\sqrt{3}}}{n-6} \tag{28a}$$

$$\lambda_{n>6} \equiv \frac{\dot{S}^{\mathrm{Tj}}_{n>6}}{\dot{S}^{\mathrm{VNM}}_{n>6}} \cong \frac{n\left(1-\frac{6}{\pi\Lambda B}\right)-6}{n-6} \tag{28b}$$

represent the ratio of the rate of grain area change for finite triple junction mobility and for the ideal vNM case. For the same value of Λ grains with $n < 6$ deviate more strongly from the ideal vNM case than do grains with $n > 6$. For example, grains with $n = 4$ are under triple junction control (Fig. 10a), while the growth of grains with n = 9 is still governed by boundary kinetics (Fig. 10b). In other words, triple junction drag does not only slow down the rate of grain growth, but also changes the grain microstructure of 2D polycrystals. This is also evident in experimental observations of grain growth in thin foils [16]. At the stage of the process where a triple junction influence becomes obvious, i.e. when the time dependency of the mean grain size is linear, the grain size distribution becomes wider.

For grain growth strictly controlled by triple junction motion, theory predicts that the grain boundaries become flat and that the grains approach a shape of equilateral polygons. A polygon of arbitrary shape will be transformed into an equilateral polygon, and any deviation from an equilateral polygon will generate a force to restore the equilibrium shape. The only exception is a triangle, i.e. a grain of topological class n

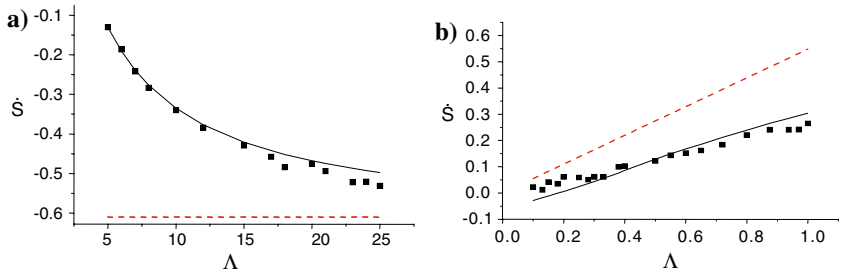

Fig. 10 The rate of grain area change $\dot{S}$ as a function of Λ. (**a**) for grains with $n = 4$. Filled squares are the results of computer simulations. The solid line represents the theoretical prediction for intermediate kinetics ($5 < \Lambda < 25$), the dotted line corresponds to the von Neumann–Mullins relation. (**b**) For grains with $n = 9$. The solid line is the theoretical prediction for intermediate kinetics, the broken line represents triple junction kinetics

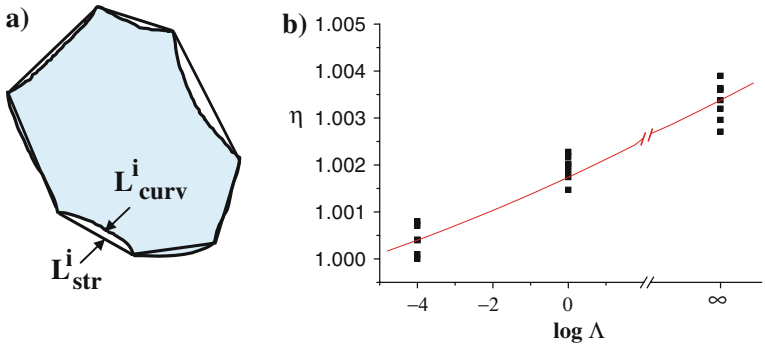

Fig. 11 Measure of boundary straightness: (**a**) diagram explaining how the value η was measured; (**b**) computer simulation (filled squares) up to $S_t/S_0 = 10$ and theoretical prediction (dash line) of $\eta(\log\Lambda)$

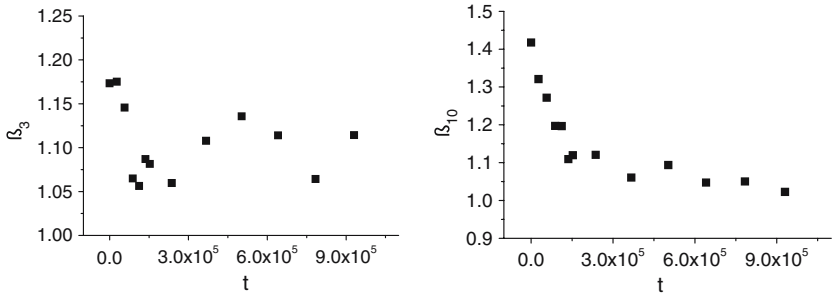

Fig. 12 Time dependence of β_n for $n = 3$ and $n = 10$ under triple junction kinetics ($\Lambda \approx 10^{-4}$) up to $S_t/S_0 = 10$.

$= 3$ is always unstable and bound to disappear. The computer simulations fully confirm the theoretical predictions. The ratio

$$\eta = \frac{\sum_{i=1}^{n} \frac{L_{curv}}{L^i_{str}}}{n} \tag{29}$$

gives a quantitative measure of grain boundary curvature, where L_{curv} is the length of a curved boundary and L_{str} is the distance between the two corresponding triple junctions (Fig. 11a). When Λ tends to zero, $\eta \to 1$ (Fig. 11b).

To assess the theoretical prediction that under triple junction kinetics all 2D grains of arbitrary shape become converted to equilateral polygons—except for triangles—we define the parameter

$$\beta_n = \frac{\frac{L_1}{L_2} + \frac{L_2}{L_3} + \cdots + \frac{L_{n-1}}{L_n} + \frac{L_n}{L_1}}{n} \tag{30}$$

where L_i is the length of the i-th side of an n-sided grain. When the shape of a grain approaches an equilateral polygon, $\beta_n \to 1$. The only exception is a triangle, which is unstable and has to disappear, i.e. β_3 should not converge toward $\beta_3 = 1$. The behavior of β_n with time was determined from the computed microstructure, including β_3 (Fig. 12). Apparently for all studied n-sided polygons $\beta_n \to 1$, except for β_3 which changes randomly.

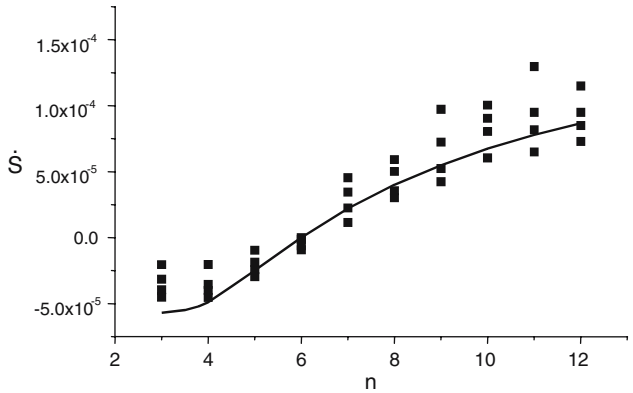

Fig. 13 $\dot{S}$ versus topological class n. Simulation results (filled squares) for $\Lambda \sim 10^{-4}$. The solid line represents the dependency predicted by Eq. (27)

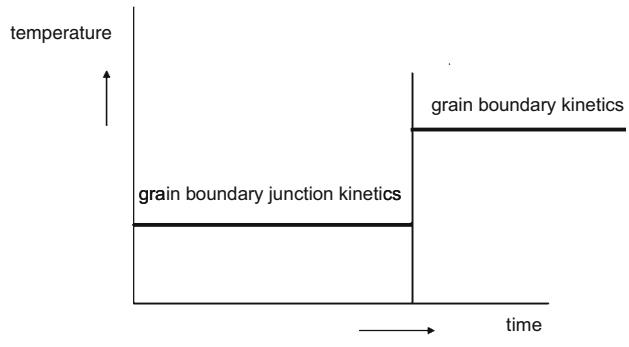

Fig. 14 Procedure of junction kinetics heat treatment (JKT): two consecutive annealings: at junction and grain boundary kinetics, respectively

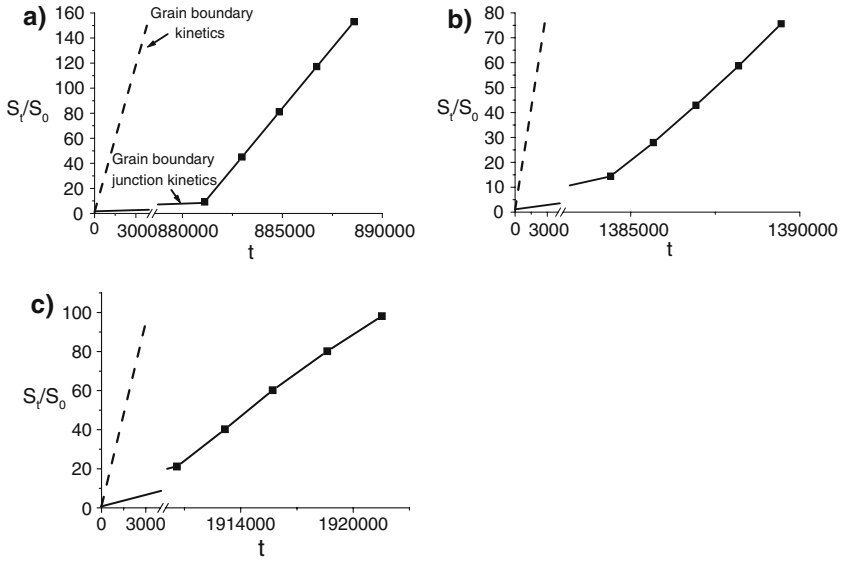

Fig. 15 The kinetics of mean grain area change for JKT: boundary kinetics (dashed line) and junction kinetics (solid line), ■-annealing at boundary kinetics after heat treatment at junction kinetics ($\Lambda = 10^{-4}$) for different starting ratio $\frac{S_t}{S_0}$: 10 (**a**); 15 (**b**); 20 (**c**) correspondingly; the time of annealing is given in the arbitrary units

The function $\dot{S}(n)$ for triple junction kinetics is presented in Fig. 13. The curve is calculated according to Eq. (27) while the symbols represent simulation results. Except for the intrinsically unstable triangular grains ($n = 3$), the theoretical predictions are in good agreement with the computer experiments. We note that $\dot{S}$ rises with n and approaches a limit (Eq. (27)) at variance with the predictions of the vNM relation.

Grain boundary junction engineering

The effects of triple junctions lend themselves to influence microstructural evolution and thus, the terminal microstructure after heat treatment during processing of a material. This is referred to as grain boundary junction engineering. In the following, we will present some cases where the effect of junctions may lead to a considerable change of microstructural evolution during grain growth.

In recent years the thermal stability of grain microstructures has attracted special attention in particular for nanocrystalline materials. To maintain the beneficial properties of a fine grained material the microstructure should be rather stable. The traditional way to stabilize grain microstructures utilizes impurity drag or Zener drag. However, both methods change the chemistry of the material and, as a consequence, its physical and mechanical properties. Besides, the efficiency of microstructure stabilization by impurities and particles is often overrated [17]. We propose another approach, which is based on the essential difference between grain microstructures formed by junction kinetics and by boundary kinetics.

Evidently, the grain microstructure obtained during grain growth governed by junction mobility differs markedly from the microstructure obtained under grain boundary kinetics. This behavior can be utilized to influence microstructural evolution during recovery, recrystallization and especially grain growth, which will be referred to as Grain Boundary Junction Engineering.

One possible way of junction kinetics treatment (JKT) is schematically depicted in Fig. 14, which shows a sequence of annealings. As detailed in [18], the annealing at a relatively low temperature initiates grain growth at triple junction kinetics, and the obtained grain microstructure resulting from this treatment is a typical ''junction'' microstructure, a system of polygonal grains which tends to assume an equilateral shape, etc. Fig. 15 presents the results of grain growth studied by computer simulations. Evidently, a subsequent annealing at boundary kinetics conditions (after junction kinetics) requires a much larger time to reach the same grain size. An increase of the effect of JKT as expressed by the grain area ratio after junction controlled growth, S_t/S_0, conspicuously delays subsequent regular grain growth under boundary kinetics.

Acknowledgments Financial assistance from the Deutsche Forschungsgemeinschaft (Grant Go/335/10) is gratefully acknowledged. The cooperation was supported by the Deutsche Forschungsgemeinschaft (DFG Grant 436 RUS 113/714/0-1(R)) and the Russian Foundation of Fundamental Research (Grant DFG-RRFI 05-02-04017).

References

1. Gottstein G, Shvindlerman LS (1999) Grain boundary migration in metals: thermodynamics, kinetics, applications. CRC Press, Baton Rouge

2. Gottstein G, Shvindlerman LS (2002) Acta Mater 50:703
3. Gottstein G, Ma Y, Shvindlerman LS (2005) Acta Mater 53:1535
4. Gottstein G, Shvindlerman LS (2005) Scripta Mater 52:863
5. Gottstein G, Shvindlerman LS (2006) Scripta Mater 54:1065
6. Galina AV, Fradkov VE, Shvindlerman LS (1987) Phys Met Metall 63:165
7. Shvindlerman LS, Gottstein G, Czubayko U, Sursaeva VG (1997). In: Terry R-McNelly (ed) Recrystallization and related phenomena. Monterey Institute of Advanced Studies, p. 255
8. Czubayko U, Sursaeva VG, Gottstein G, Shvindlerman LS (1998) Acta mater 46:5863
9. Gottstein G, King AH, Shvindlerman LS (2000) Acta mater 48:397
10. Von Neumann J (1952) Metal interfaces. American Society for Testing Materials, Cleveland, p. 1108
11. Mullins WW (1956) J Appl Phys 27:900
12. Gottstein G, Shvindlerman LS (2005) Mat Sci Technol 21:1261
13. Kawasaki K, Nagai T, Nakashima K (1989) Philos Magn 60:399
14. Weygand D, Brechet Y (1998) Philos Magn B 78:329
15. Zheng M, Gottstein G (2002) Aluminium 78:878
16. Novikov V Yu, (2004) Mat Science Forum 467–470; 1093–1098.
17. Shvindlerman LS,Gottstein GZ (2004) Metallk 95:239